

Magnetar giant flare origin for GRB 200415A inferred from a new scaling relation

Hai-Ming Zhang^{1,2}, Ruo-Yu Liu^{1,2}, Shu-Qing Zhong^{1,2} and Xiang-Yu Wang^{1,2}

¹School of Astronomy and Space Science, Nanjing University, Nanjing 210093, China

²Key laboratory of Modern Astronomy and Astrophysics, Nanjing University, Ministry of Education, Nanjing 210093, China

xywang@nju.edu.cn; ryliu@nju.edu.cn

Soft gamma-ray repeaters (SGRs) are mainly a Galactic population and originate from neutron stars with intense ($B \simeq 10^{15}$ G) magnetic fields (magnetars). Occasionally (once every 30 – 40 yr), a giant flare occurs with enormous intensity, displaying a short hard spike, followed by a weaker, oscillatory phase which exhibits the period of the neutron star. If the magnetar giant flares occur in nearby galaxies, they would appear as cosmic short-hard gamma-ray bursts (GRBs) without detecting the weak oscillatory phase. Recently, a short-hard GRB named GRB 200415A was detected, with a position coincident with the Sculptor Galaxy (NGC 253), raising the question whether it is a classic short GRB or a magnetar giant flare. Here we show that magnetar giant flares follow a scaling relation between the spectral peak energy and the isotropic energy in 1 keV – 10 MeV, i.e., $E_p \propto E_{\text{iso}}^{1/4}$, and locate in a distinct region of the $E_p - E_{\text{iso}}$ plane from that of classic short GRBs. The relation can be well understood in the model that giant flares arise from the photosphere emissions of relativistically expanding fireball. GRB 200415A, together with two other candidate giant flares (GRB 051103 and GRB 070201) follow this relation, which strongly favor the giant flare origin of these GRBs. The GeV emission detected by *Fermi*/LAT from GRB 200415A at 18 – 285 s can also be explained in the giant flare scenario. The total energy in the GeV emission implies a baryon load of $\sim 10^{23}$ g in the giant flare fireball of GRB 200415A.

Soft gamma-ray repeaters (SGRs) are a special rare class of slowly rotating, strongly magnetized neutron stars dubbed “magnetar”¹. They emit repeating bursts through magnetic energy dissipation, and occasionally release a giant flare (GF) with enormous intensity, which display a short hard spike followed by a soft oscillating tail (e.g. ref.²). So far, there are four GFs that have been detected. GRB 790305 is the first GF detected from SGR 0526-66^{3,4}. After ~ 20 years later, three more GFs were detected, GRB 980618 from SGR 1627-41^{5,6}, GRB 980827 from SGR 1900+14⁷⁻⁹, and GRB 041227 from SGR 1806-20^{10,11}. These events are now considered to be a very rare type of astrophysical phenomenon and completely different from classic short gamma-ray bursts (GRBs), which result from mergers of compact objects and occur at cosmological distance typically.

On the other hand, however, if a magnetar giant flare occurs in an external galaxy, only the initial peak of a GF would be detectable, and thus the GF would resemble a several hundred millisecond long, hard-spectrum GRB¹⁰. Indeed, two candidate giant flares have been suggested, i.e., GRB 051103, spatially coincident with the galaxy M81¹², and GRB 070201, coincident with the galaxy M31¹³. The chance coincidence probability between the IPN localization of GRB 051103 (and GRB 070201) and a nearby galaxy is low ($\sim 1\%$)¹⁴. At 08:48:05.56 UT

on 15 April 2020, the Fermi Gamma-Ray Burst Monitor (GBM) triggered and located GRB 200415A, which was also detected by *Fermi*/LAT^{15–17}. Interestingly, the burst is localized by the IPN and the localization (a 274 arcmin² error box) shows that the Sculptor Galaxy (NGC 253) is inside the IPN box¹⁸. Thus, it is possible that GRB 200415A is a GF from the Sculptor Galaxy^{18–20}. However, without identifying the oscillatory phase or SGR activity, these candidates can not be confirmed reliably to be true GFs.

We analyzed the *Fermi*/GBM data of GRB 200415A (see the Method). The burst exhibits the common temporal characteristics of GFs, i.e., a short initial pulse (~ 168 ms) with a steep leading edge (≤ 6 ms) and a quasi-exponential decay ($\tau = 42.5$ ms)^{9,13,21,22}. We then extract the time integrated spectrum during the peak period (i.e., from $T_0 - 0.010$ to $T_0 + 0.158$ s). We find that the spectrum can be successfully fitted by a power law function with an exponential high-energy cutoff (hereafter, cutoff power law or CPL model). The power law index is $-0.05_{-0.10}^{+0.10}$ and the cutoff energy, parameterized as E_p , is $916.3_{-112.8}^{+124.5}$ keV. The average flux in this time interval is $(5.08 \pm 0.56) \times 10^{-5}$ erg cm⁻² s⁻¹ (between 1 keV and 10 MeV) and the total fluence is $(8.53 \pm 0.94) \times 10^{-6}$ erg cm⁻². Assuming that the source of GRB 200415A is situated in NGC 253 at a distance of 3.5 Mpc, the measured value of the fluence corresponds to a total isotropic energy is $(1.25 \pm 0.13) \times 10^{46}$ erg. We found that the spectrum displayed a strong hard-to-soft spectral evolution, which is consistent with the spectral characteristics of both GFs and GRBs.

The spectral peak energy and the total isotropic energy of GRB 200415A, together with four GFs and two GF candidates, are summarized in Table 1. With the observed properties of these magnetar GFs and candidates, we find an interesting relation between the peak energy E_p and the isotropic energy E_{iso} of them. We first use the four identified GFs for the study. The best-fit relation between the peak energy E_p and the total isotropic energy E_{iso} of the four GFs is $\log(E_p/\text{keV}) = (2.88 \pm 0.20) + (0.24 \pm 0.10) \log(E_{\text{iso}}/10^{46}\text{erg})$, with a Pearson correlation coefficient of $\kappa = 0.94$ and a chance probability of $p = 0.06$. As shown in Figure 1, plotting GRB 200415A onto the E_p vs. E_{iso} plane, we find that GRB 200415A is in perfect agreement with this relation and far away from the short GRB population. This indicates that GRB 200415A is more likely to be a magnetar GF from the Sculptor Galaxy (see Supplement Fig. S1 for more information).

Considering also the other two candidate GFs (GRB 051103 and GRB 070201) lying within the 1σ of the track of the GF population, we include these three candidates to do the re-fitting. We find that the best-fit relation gives a tighter relation: $\log(E_p/\text{keV}) = (2.84 \pm 0.12) + (0.25 \pm 0.08) \log(E_{\text{iso}}/10^{46}\text{erg})$, with a Pearson correlation coefficient of $\kappa = 0.93$ and a chance probability of $p = 0.002$. This correlation suggests that these candidate GFs and four identified GFs belong to the same class of sources. This relation is quite different from the correlation for short GRBs, namely, the "Amati relation" (ref.²³; $\log(E_{p,z}/\text{keV}) = (3.55 \pm 0.07) + (0.54 \pm 0.04) \log(E_{\text{iso}}/10^{52}\text{erg})$, where $E_{p,z} = E_p(1+z)^1$). As shown in Figure 1, GFs lie outside of the 3σ region of the Amati relation for short GRBs. We also find that the two correlations do not agree at $> 5\sigma$ level, indicating that GFs are distinct from short GRBs.

Next we show that the correlation between E_p and E_{iso} for magnetar GFs can be understood in the framework of the fireball photosphere emission model. During a GF, strong shearing of a neutron star's magnetic field, combined with growing thermal pressure, appears to have

¹The short GRBs data obtained from ref. ²⁴

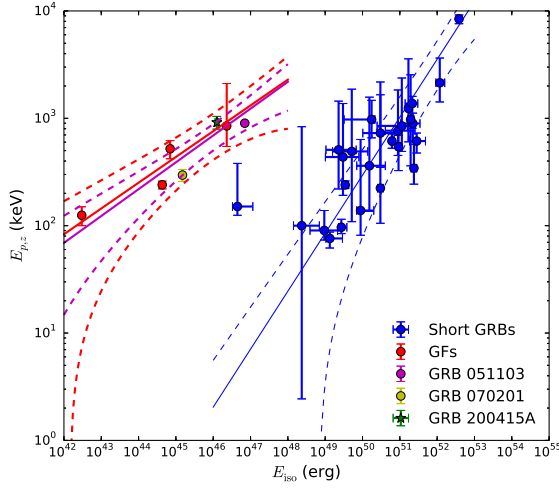


Figure 1: GRB 200415A in the $E_{p,z}$ - E_{iso} correlation diagram. The blue data points represent short GRBs taken from ²⁴. The GFs (red) and candidates (yellow and magenta) marked as the color data points are derived from the references as shown in Table 1. The solid lines are the best fit correlations: $\log(E_{p,z}/\text{keV}) = (3.55 \pm 0.07) + (0.54 \pm 0.04) \log(E_{\text{iso}}/10^{52}\text{erg})$ for short GRBs (blue line), $\log(E_{p,z}/\text{keV}) = (2.88 \pm 0.20) + (0.24 \pm 0.10) \log(E_{\text{iso}}/10^{46}\text{erg})$ for four established GFs (red line), and $\log(E_{p,z}/\text{keV}) = (2.84 \pm 0.12) + (0.25 \pm 0.08) \log(E_{\text{iso}}/10^{46}\text{erg})$ for considering the GFs and three candidates (magenta line; including GRB 051103, 070201 and 200415A). The blue dashed line represents the 3σ region of the correlation, and the magenta and red dashed lines represent 1σ regions of the correlation. The green star represents the GRB 200415A.

Table 1: Properties of magnetar GFs and Candidates

GRB	SGR or associated galaxy	D_L kpc	E_{iso} erg	E_p keV
790305 ^a	SGR 0526–66 (LMC)	50	7.0×10^{44}	520.0 ± 100.0
980618 ^b	SGR 1627–41	5.8	3.0×10^{42}	125.0 ± 25.0
980827 ^c	SGR 1900+14	15	4.3×10^{44}	240.0 ± 20.0
041227 ^d	SGR 1806–20	15	2.3×10^{46}	$850.0_{-303.0}^{+1259.0}$
051103 ^e	M81	3600	7.0×10^{46}	~ 900.0
070201 ^f	M31	780	1.5×10^{45}	$296.0_{-32.0}^{+38.0}$
200415A ^g	Sculptor Galaxy (NGC 253)	3500	$(1.25 \pm 0.13) \times 10^{46}$	$916.3_{-112.8}^{+124.5}$

a ref.^{13,21}

b ref.⁵

c ref.^{7,25}

d ref.¹¹

e ref.^{13,22}

f ref.¹³

g this work

forced an opening of the field outward²⁷. A huge amount of magnetic energy $E = 10^{46}$ erg is subsequently released at the surface of the neutron star with a radius of R_0 over a short period of $t = 0.1$ s, leading to the formation of a hot fireball^{26–28}, which is quite similar to the case of classic GRBs²⁹. The optical depth for pair production is extremely high, regardless of the suppression of the effective cross-section due to the large magnetic field of the magnetar³⁰. With such a large optical depth, a radiation-pairs plasma is formed at a thermal equilibrium with an initial temperature

$$kT_0 = \left(\frac{E}{4\pi R_0^2 \sigma t} \right)^{1/4} = 200 \text{ keV} E_{46}^{1/4} R_0^{-1/2} t_{-1}^{-1/4}, \quad (1)$$

where σ is the Stephan-Boltzmann constant. This plasma expands under its own pressure, launching a relativistic outflow. As the optically thick (adiabatic) outflow expands, the comoving internal energy drops as $e' \propto V^{-4/3} \propto n'^{4/3}$, where n' is the comoving baryon number density. The baryon bulk Lorentz factor increases as $\Gamma \propto R$ and the comoving temperature drops $T' \propto R^{-1}$ (e.g. ref.³¹). The e^\pm pairs drop out of equilibrium^{32,33} at $T'_p = 17$ KeV at a radius of $R_p = R_0(T_0/T'_p)$. This is the radius of an e^\pm pair photosphere. If the outflow carries enough baryons, the baryonic electrons lead to a photosphere larger than R_p . As long as the outflow remains optically thick, it is radiation dominated and continues to expand with $\Gamma \propto R$. For large baryon loads, Γ reaches the saturation value η at a radius $R_s = \eta R_0$, where the baryon load is parameterized by $\eta = E/Mc^2$. Above the saturation radius, the flow continues to coast with $\Gamma = \eta$.

On the other hand, for low baryon loads, a baryonic electron photosphere appears in the accelerating portion $\Gamma \propto R$. An electron scattering photosphere is defined by $\tau = \sigma_T n' R_{ph} / \Gamma = 1$, where $n' = (L/4\pi m_p c^3 \Gamma \eta)$ is the comoving baryon density and r/Γ is a typical comoving

length. There is a critical value of η at which $R_{ph} = R_s$, i.e.,

$$\eta_* = \left(\frac{L\sigma_T}{4\pi m_p c^3 R_0} \right)^{1/4} = 100 L_{47}^{1/4} R_{0,6}^{-1/4}. \quad (2)$$

Thus, for low baryon loads where $\eta \geq \eta_*$, the outflow becomes optically thin in the accelerating portion. The outflow emits a quasi-blackbody spectrum as it became optically thin, with a spectral temperature comparable to the temperature at its base, because declining temperature in the outflow is compensated by the relativistic blueshift, i.e., $T_{ph} = \Gamma T'_{ph} = T_0$. The observed photospheric thermal luminosity is $L_{ph} = 4\pi R^2 \Gamma^2 \sigma T_{ph}^4 = 4\pi R_0^2 \sigma T_{ph}^4$. Thus, the observer-frame photospheric temperature is

$$kT_{ph} = \left(\frac{E_{iso}}{4\pi R_0^2 \sigma t} \right)^{1/4} = 200 \text{ KeV } E_{iso,46}^{1/4} R_0^{-1/2} t_{-1}^{-1/4}, \quad (3)$$

where $E_{iso} = L_{ph} t$ and we have assumed a duration of $t = 0.1$ s for the all the GFs. The peak energy of the spectrum is at $E_p = 2.8 kT_{ph}$. It is remarkable to see that Eq.(3) agrees well with the $E_p - E_{iso}$ relation that we found for GFs.

The spectra of GRB 200415A and some other GFs are not purely blackbody and better modelled by CPL spectrum. This can be interpreted as being due to the extra contribution by some other radiation components to the low-energy spectrum, such as multi-temperature blackbody emission or synchrotron emission arising from some shocks in the relativistic outflow. There is evidence for multi sub-pulses and fast variability in the initial spike in this and other GFs. Different sub-pulses have different temperatures, so multi-temperature blackbody is naturally expected. The fast variability implies unsteady outflow, so internal shocks could occur, which may produce a flat synchrotron spectrum. If this synchrotron spectrum is subdominant compared with the photosphere emission, the low-energy spectrum will be flatter while the peak energy remains unchanged²⁹. A detailed study of the spectrum considering these effects is beyond the scope of the present paper.

Note that Eq.(3) holds only when $R_{ph} < R_s$, corresponding to $\eta > \eta_*$. If $R_{ph} > R_s$ ($\eta < \eta_*$), the observer-frame photospheric temperature and photospheric thermal luminosity evolve as $T_{ph} \propto R^{-2/3}$ and $L_{ph} \propto R^{-2/3}$, respectively. In this case, the relation is different from Eq.(3). This implies that baryon load in the outflow of GRB 200415A should satisfy the condition $\eta > \eta_*$.

The outflow reaches a Lorentz factor of $\Gamma = R_{ph}/R_0 = \eta_*(\eta/\eta_*)^{-1/3}$ at the photosphere. Beyond the photosphere, most of the electrons above the photosphere can still scatter with a decreasing fraction of free-streaming photons as long as the comoving Compton drag time is less than the comoving expansion time²⁹. As a result, for $\eta > \eta_*$, the terminal Lorentz factor of the outflow is η_* (instead of η). The energy that remains in the baryons of the outflow is $E_b = E(\eta_*/\eta)$. For magnetar GFs, as $\eta > \eta_*$, we expect $E_b < E$. The energy in the afterglow emission of GFs could place a limit on the energy in the final baryonic ejecta. The fluence of the GeV emission of GRB 200415A is about $(2.9 \pm 0.2) \times 10^{-6}$ erg cm² in the time interval 0 – 300 s, which is only a factor of 3 smaller than the fluence of the GF (see the Method). This implies that η should not be much larger than η_* . As a result, we estimate that the baryon load in the GF of GRB 200415A is about $M = E/(\eta c^2) \sim 10^{23}$ g.

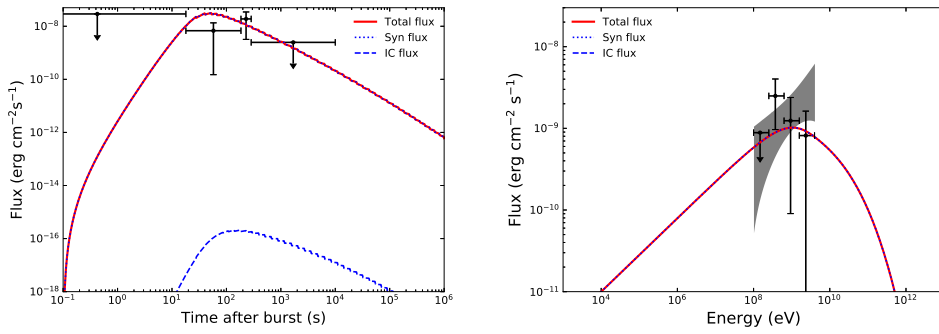


Figure 2: Left panel: modeling of the light curve of the GeV emission of GRB 200415A. The dotted curve and dashed curve represent the synchrotron component and SSC component, respectively. Right panel: modeling of the spectrum of the GeV emission of GRB 200415A at $t = 18\text{--}185$ s. The black data points represent the GeV flux spectra of GRB 200415A. The grey butterfly shows the best fit power-law model with 1σ error. The parameters used in the fitting are $E = 1.25 \times 10^{46}$ erg, $n = 1 \times 10^{-5}$ cm $^{-3}$, $\epsilon_e = 0.95$, $\epsilon_B = 0.08$, $\Gamma_0 = 100$, and $p = 2.1$.

While GeV afterglow emission is commonly seen in short GRBs, it can not be taken as evidence against the magnetar GF origin. Indeed, GRB200415A is the first GF observed by Fermi/LAT, which has started operation since 2008. We suggest that the GeV emission may be produced by the shocks arising from the interaction between the relativistic outflow and the ambient medium. Generally there are two shocks, one is the forward shock expanding into the ambient medium and the other is the reverse shock expanding into the outflow ejecta. Both shocks could accelerate electrons, producing synchrotron emission and inverse-Compton emission. Below we study the possibility of the forward shock emitting the GeV afterglow emission. Since the terminal Lorentz factor of the relativistic outflow after the acceleration is η_* , we take $\Gamma_0 = 100$ as a reference value for the initial Lorentz factor of the forward shock. The modeling results of the afterglow light curve and SED for GRB 200415A are shown in Figure 2. The low density of the ambient medium is not surprising, since the pulsar wind and earlier SGR activity from the magnetar may have created a cavity around the pulsar. Indeed, it has been suggested that the Poynting flux emanating from the pulsar can excavate a bow-shock cavity around the pulsar with a size as large as fractions of a parsec³⁸. The value of the electron equipartition factor $\epsilon_e = 0.95$ seems to be higher than that inferred for classic GRBs, but considering that the ambient medium around the pulsar may be enriched with pairs, such a value of ϵ_e may be reasonable for magnetar GFs³⁹.

To summarize, we have shown that magnetar GFs locate in a distinct region of the $E_p - E_{\text{iso}}$ plane and follow a scaling relation roughly as $E_p \propto E_{\text{iso}}^{1/4}$, quite different from those of classic short GRBs. Although the number of GFs in our sample is small, the scaling relation is well consistent with the expectation of the fireball model of magnetar GFs, which explains GFs as the photospheric emission of hot fireballs formed as a result of catastrophic instabilities in magnetars²⁷. This scaling relation thus provides a useful tool to distinguish between magnetar GFs and classic short GRBs. Along this line, we suggest that GRB 200415A is a magnetar GF occurred in the nearby galaxy NGC 253.

Methods

GBM Data Reduction and Analysis.

GRB 200415A triggered *Fermi*/GBM at 08:48:05.56 UT on 15 April 2020 (T_0)¹⁶. This GRB was also detected by Konus/Wind¹⁹ and INTEGRAL²⁰. And ref.¹⁸ found that the IPN localization is consistent with and smaller than the area of the Fermi-GBM final position¹⁵ and BALROG localization⁴⁰.

The GBM data of GRB 200415A is downloaded from the public science support center at the official Fermi Web site². We select the trigger detectors, e.g., NaI detectors n0 & n1 and BGO detector b0. The software package XSPEC (version 12.10) is used for performing the spectral fitting. We first extract the time integrated spectrum in the peak region (i.e., from $T_0 - 0.010$ to $T_0 + 0.158$ s) by a power law function with an exponential high-energy cutoff. Then, we divided this time interval into three segments to study its spectral evolution. We also tested the Band function model that are usually used in classic gamma-ray bursts (Band function⁴²) in the spectral analysis. We found that it can also fit the spectrum, but no statistically significant high-energy power-law tail is found ($\beta < -2.95$ is not constrained well). To check whether the Band function fit is overfitting (since it has one extra parameter), we employ a Bayesian information criterion (BIC⁴³) to check its statistical confidence. The comparison of the two models leads to $\Delta BIC = 5.66$ (Band function model has the higher BIC). As suggested by ref.⁴¹, such a ΔBIC value indicates positive evidence against the higher BIC model, i.e., the Band function model. Therefore, we favorably choose the cutoff power law model as the best-fit model in our analysis for this GRB.

Temporal characteristics is another important feature of GFs. The light curve of GRB 200415A observed in the GBM energy range (8–40,000 keV) with a time resolution of 2 ms is shown in Supplementary Figure S2 on semilogarithmic scale. We fit the light curve with a quasi-exponential function (e.g. $N(t) = N_0 \exp(-t/\tau) + N_{bkg}$) in the decay phase, and find that it shows a quasi-exponential decay with $\tau = 42.5$ ms.

LAT Data Reduction and Analysis.

Remarkably, this event was detected by *Fermi*/LAT in the GeV band¹⁷. The *Fermi*/LAT data for the GRB 200415A was taken from the Fermi Science Support Center³. The data analysis was performed using the publicly available software *fermitools* (ver. 1.0.0) with the unbinned likelihood analysis method. Using the tool *gfndsrc* and assuming a power-law spectrum of the burst, we estimated the best-fit *Fermi*/LAT position of GRB 200415A is (11.10deg, -25.03deg), with circular errors of 0.41deg and 0.68 deg (statistical only), respectively at 68% and 90% confidence levels. The *P8R3_TRANSIENT020_V2* set of instrument response functions (IRFs) is used. Since the highest-energy photon of GRB 200415A is a 1.72 GeV event, which is observed 284 seconds after the GBM trigger, we only consider the events with energies from 100 MeV to 10 GeV. Taking into the consideration of the background point-like sources, Galactic diffuse and isotropic emission, we found the test statistic (TS) of the burst is 35.9 ($\sim 6\sigma$) at T_0 to $T_0 + 300$ s. The TS value is defined as $TS = 2(\ln \mathcal{L}_1 - \ln \mathcal{L}_0)$, where \mathcal{L}_0 is the likelihood of background (null hypothesis) and \mathcal{L}_1 is the likelihood of the hypothesis for adding the burst. The averaged flux is $(9.52 \pm 0.61) \times 10^{-9}$ erg cm⁻² s⁻¹ with a photon index -1.46 ± 0.37 .

²<https://fermi.gsfc.nasa.gov/ssc/data/>

³<https://fermi.gsfc.nasa.gov>

As shown in Supplementary Figure S4, we compare the localization of LAT for GRB 200415A with the IPN error box and the position of NGC 253 (4FGL J0047.5–2517). We find that NGC 253 is located inside the IPN error box, and the error box center is offset by 5.93 arcmin from NGC 253. The IPN error box is inside the region of the localization contours of GRB 200415A at the 90% confidence level.

Modelling of the GeV afterglow.

We perform modeling of the *Fermi*/LAT data for GRB 200415A using the numerical code^{36,37}. According to the standard afterglow model^{34,35}, the light curve for a given observed frequency (ν) could be calculated as $F(t, \nu) = F(t, \nu, E_k, n, p, \varepsilon_e, \varepsilon_B, \Gamma_0)$, employing a numerical code developed in our previous work^{36,37}. E_k is the isotropic kinetic energy of the GRB outflow, n is the particle number density of the ambient medium, p is the electron spectral index, ε_e and ε_B are the equipartition factors for the energy in electrons and magnetic field in the shock, and Γ_0 is the initial Lorentz factor of the outflow.

1. Duncan, R. C., Thompson, C. 1992. Formation of Very Strongly Magnetized Neutron Stars: Implications for Gamma-Ray Bursts. *The Astrophysical Journal* 392, L9.
2. Palmer, D. M. and 27 colleagues 2005. A giant γ -ray flare from the magnetar SGR 1806 - 20. *Nature* 434, 1107-1109.
3. Mazets, E. P., Golentskii, S. V., Ilinskii, V. N., Aptekar, R. L., Guryan, I. A. 1979. Observations of a flaring X-ray pulsar in Dorado. *Nature* 282, 587-589.
4. Cline, T. L. and 9 colleagues 1980. Detection of a fast, intense and unusual gamma-ray transient.. *The Astrophysical Journal* 237, L1-L5.
5. Mazets, E. P. and 7 colleagues 1999. Unusual Burst Emission from the New Soft Gamma Repeater SGR 1627-41. *The Astrophysical Journal* 519, L151-L153.
6. Hurley, K. and 7 colleagues 1999. Precise Interplanetary Network Localization of a New Soft Gamma Repeater, SGR 1627-41. *The Astrophysical Journal* 519, L143-L145.
7. Hurley, K. and 13 colleagues 1999. A giant periodic flare from the soft γ -ray repeater SGR1900+14. *Nature* 397, 41-43.
8. Feroci, M. and 6 colleagues 1999. A Giant Outburst from SGR 1900+14 Observed with the BeppoSAX Gamma-Ray Burst Monitor. *The Astrophysical Journal* 515, L9-L12.
9. Mazets, E. P. and 7 colleagues 1999. Activity of the soft gamma repeater SGR 1900 + 14 in 1998 from Konus-Wind observations: 2. The giant August 27 outburst. *Astronomy Letters* 25, 635-648.
10. Hurley, K. and 19 colleagues 2005. An exceptionally bright flare from SGR 1806-20 and the origins of short-duration γ -ray bursts. *Nature* 434, 1098-1103.
11. Frederiks, D. D. and 7 colleagues 2007. Giant flare in SGR 1806-20 and its Compton reflection from the Moon. *Astronomy Letters* 33, 1-18.

12. Golenetskii, S. and 31 colleagues 2005. IPN triangulation and konus spectrum of the bright short/hard GRB051103.. GRB Coordinates Network, Circular Service, No. 4197, #1 (2005) 4197.
13. Mazets, E. P. and 8 colleagues 2008. A Giant Flare from a Soft Gamma Repeater in the Andromeda Galaxy (M31). *The Astrophysical Journal* 680, 545-549.
14. Svinkin, D. S.; Hurley, K.; Aptekar, R. L.; Golenetskii, S. V.; Frederiks, D. D., 2015, A search for giant flares from soft gamma-ray repeaters in nearby galaxies in the Konus-WIND short burst sample. *Monthly Notices of the Royal Astronomical Society*, 447, Issue 1, 1028-1032
15. Bissaldi, E., Briggs, M., Burns, E., Roberts, O. J., Veres, P., Fermi GBM Team 2020. GRB 200415A: Fermi GBM observation. GRB Coordinates Network, Circular Service, No. 27587 27587.
16. Fermi GBM Team 2020. GRB 200415A: Fermi GBM Final Real-time Localization. GRB Coordinates Network, Circular Service, No. 27579 27579.
17. Omodei, N. and 7 colleagues 2020. GRB 200415A: Fermi-LAT detection. GRB Coordinates Network, Circular Service, No. 27586 27586.
18. Svinkin, D. and 35 colleagues 2020. Improved IPN error box for GRB 200415A (consistent with the Sculptor Galaxy). GRB Coordinates Network, Circular Service, No. 27595 27595.
19. Frederiks, D. and 9 colleagues 2020. Konus-Wind observation of GRB 200415A (a magnetar Giant Flare in Sculptor Galaxy?). GRB Coordinates Network, Circular Service, No. 27596 27596.
20. Pozanenko, A., Minaev, P., Chelovekov, I., Grebenev, S. 2020. GRB 200415A (possible magnetar Giant Flare in Sculptor Galaxy): INTEGRAL observations. GRB Coordinates Network, Circular Service, No. 27627 27627.
21. Mazets, E. P., Golenetskii, S. V., Gurian, I. A., Ilinskii, V. N. 1982. The 5 March 1979 event and the distinct class of short gamma bursts: are they of the same origin?. *Astrophysics and Space Science* 84, 173-189.
22. Frederiks, D. D., Palshin, V. D., Aptekar, R. L., Golenetskii, S. V., Cline, T. L., Mazets, E. P. 2007. On the possibility of identifying the short hard burst GRB 051103 with a giant flare from a soft gamma repeater in the M81 group of galaxies. *Astronomy Letters* 33, 19C24.
23. Amati, L. and 15 colleagues 2002. Intrinsic spectra and energetics of BeppoSAX Gamma-Ray Bursts with known redshifts. *Astronomy and Astrophysics* 390, 81-89.
24. Zhang, B.-B. and 17 colleagues 2018. A peculiar low-luminosity short gamma-ray burst from a double neutron star merger progenitor. *Nature Communications* 9.

25. Tanaka, Y. T. and 7 colleagues 2007. Comparative Study of the Initial Spikes of Soft Gamma-Ray Repeater Giant Flares in 1998 and 2004 Observed with Geotail: Do Magnetospheric Instabilities Trigger Large-Scale Fracturing of a Magnetar's Crust?. *The Astrophysical Journal* 665, L55-L58.
26. Thompson, C.; Duncan, R. C. 1995. The soft gamma repeaters as very strongly magnetized neutron stars - I. Radiative mechanism for outbursts. *Monthly Notices of the Royal Astronomical Society*, 275, pp. 255-300.
27. Thompson, C., Duncan, R. C. 2001. The Giant Flare of 1998 August 27 from SGR 1900+14. II. Radiative Mechanism and Physical Constraints on the Source. *The Astrophysical Journal* 561, 980-1005.
28. Nakar, E., Piran, T., Sari, R. 2005. Pure and Loaded Fireballs in Soft Gamma-Ray Repeater Giant Flares. *The Astrophysical Journal* 635, 516-521.
29. Mészáros, P., Rees, M. J. 2000. Multi-GEV Neutrinos from Internal Dissipation in Gamma-Ray Burst Fireballs. *The Astrophysical Journal* 541, L5-L8.
30. Herold, H. 1979. Compton and Thomson scattering in strong magnetic fields. *Physical Review D* 19, 2868-2875.
31. Shemi, A., Piran, T. 1990. The Appearance of Cosmic Fireballs. *The Astrophysical Journal* 365, L55.
32. Paczynski, B. 1986. Gamma-ray bursters at cosmological distances. *The Astrophysical Journal* 308, L43-L46.
33. Paczynski, B. 1990. A Test of the Galactic Origin of Gamma-Ray Bursts. *The Astrophysical Journal* 348, 485.
34. Mészáros, P., Rees, M. J. 1997. Optical and Long-Wavelength Afterglow from Gamma-Ray Bursts. *The Astrophysical Journal* 476, 232-237.
35. Sari, R. 1997. Hydrodynamics of Gamma-Ray Burst Afterglow. *The Astrophysical Journal* 489, L37-L40.
36. Liu, R.-Y., Wang, X.-Y., Wu, X.-F. 2013. Interpretation of the Unprecedentedly Long-lived High-energy Emission of GRB 130427A. *The Astrophysical Journal* 773.
37. Wang, X.-Y., Liu, R.-Y., Zhang, H.-M., Xi, S.-Q., Zhang, B. 2019. Synchrotron Self-Compton Emission from External Shocks as the Origin of the Sub-TeV Emission in GRB 180720B and GRB 190114C. *The Astrophysical Journal* 884.
38. Holcomb, C., Ramirez-Ruiz, E., De Colle, F., Montes, G. 2014. Diversity of Short Gamma-Ray Burst Afterglows from Compact Binary Mergers Hosting Pulsars. *The Astrophysical Journal* 790.
39. Königl, A., Granot, J. 2002. Gamma-Ray Burst Afterglows in Pulsar-Wind Bubbles. *The Astrophysical Journal* 574, 134-154.

40. Kunzweiler, F., Biltzinger, B., Berlato, F., Greiner, J. B., J. 2020. GRB 200415A: BALROG localization (Fermi Trigger 608633290 / GRB 200415367). GRB Coordinates Network, Circular Service, No. 27580 27580.
41. Lü, H.-J. and 8 colleagues 2017. Extremely Bright GRB 160625B with Multiple Emission Episodes: Evidence for Long-term Ejecta Evolution. *The Astrophysical Journal* 849.
42. Band, D. and 14 colleagues 1993. BATSE Observations of Gamma-Ray Burst Spectra. I. Spectral Diversity. *The Astrophysical Journal* 413, 281.
43. Schwarz, G. Estimating the Dimension of a Model. *Ann. Stat.* **6**, 461-464 (1978)
44. Pence, W. D. 1980. A photometric and kinematic study of the barred spiral galaxy NGC 253. I - Detailed surface photometry.. *The Astrophysical Journal* 239, 54-64.

Acknowledgments

This work has made use of data and software provided by the Fermi Science Support Center. X.Y.W. is supported by the National Key R & D program of China under the grant 2018YFA0404200 and the NSFC grants 11625312 and 11851304.

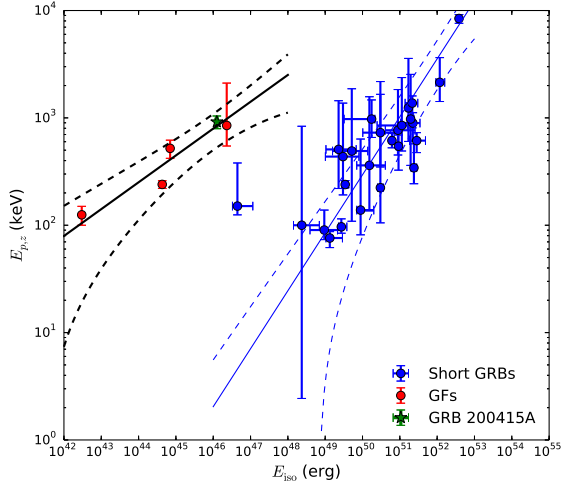


Figure S1: The same as Figure 1, but for the fitting of four GFs and GRB 200415A. The black solid line is the best fit and represents the correlation: $\log(E_{p,z}/\text{keV}) = (2.90 \pm 0.16) + (0.25 \pm 0.09) \log(E_{\text{iso}}/10^{46}\text{erg})$. The blue dashed line represents the 3σ region of the correlation, and the black dashed line represents 1σ region of the correlation.

Table S1: Spectral Fitting Results of GRB 200415A

Time Interval	Cutoff Power-Law Fitting				Band Fitting				Model Comparison	
	α	E_p (keV)	$\frac{\text{PGSLAT}}{\text{dof}}$	BIC	α	β	E_p (keV)	$\frac{\text{PGSLAT}}{\text{dof}}$		BIC
-0.010 ~ 0.158	$-0.05^{+0.10}_{-0.10}$	$916.3^{+124.5}_{-112.8}$	327.83/359	345.51	$0.09^{+0.15}_{-0.14}$	< -2.95	$834.5^{+183.3}_{-150.1}$	327.60/358	351.17	5.66
-0.010 ~ 0.046 (a)	$-0.05^{+0.10}_{-0.11}$	$1040.3^{+140.9}_{-127.9}$	350.29/359	367.96	$0.05^{+0.11}_{-0.10}$	< -3.69	$1040.3^{+142.5}_{-129.1}$	350.06/358	373.63	5.67
0.046 ~ 0.102 (b)	$-0.33^{+0.27}_{-0.32}$	$489.1^{+169.1}_{-143.4}$	355.15/359	372.82	$0.36^{+0.32}_{-0.28}$	< -2.82	$465.1^{+178.5}_{-132.1}$	354.94/358	378.51	5.69
0.102 ~ 0.158 (c)	$-0.70^{+0.58}_{-0.77}$	$175.0^{+152.3}_{-99.3}$	322.36/359	340.03	$4.04^{+1.04}_{-0.96}$	$-1.89^{+0.22}_{-0.33}$	$71.2^{+149.3}_{-43.5}$	317.17/358	340.74	0.71

Supplementary Information

1. Temporal and spectral analysis of GRB 200415A.

2. *Fermi*/LAT observations of GRB 200415A and localization by the IPN.

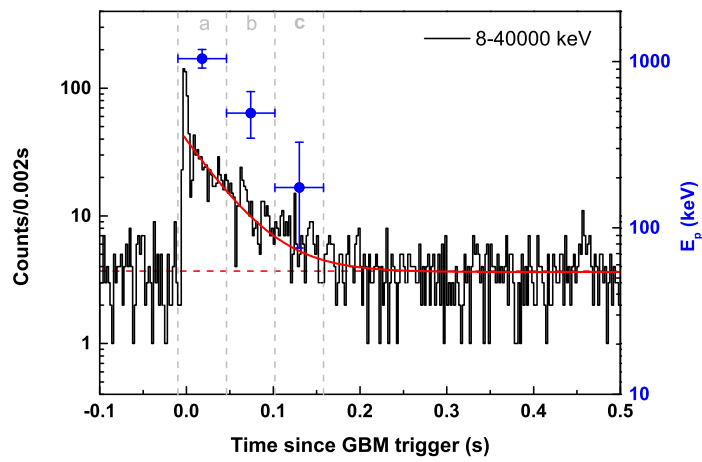


Figure S2: Light curve and E_p evolution of GRB 200415A in the GBM energy range (8–40,000 keV) on semilogarithmic scale. The red dashed line indicate the background counts. The burst decays quasi-exponentially. The red line corresponds to $\tau = 42.5$ ms. The gray dashed lines indicate the three intervals where the energy spectra were measured as shown in Table S1.

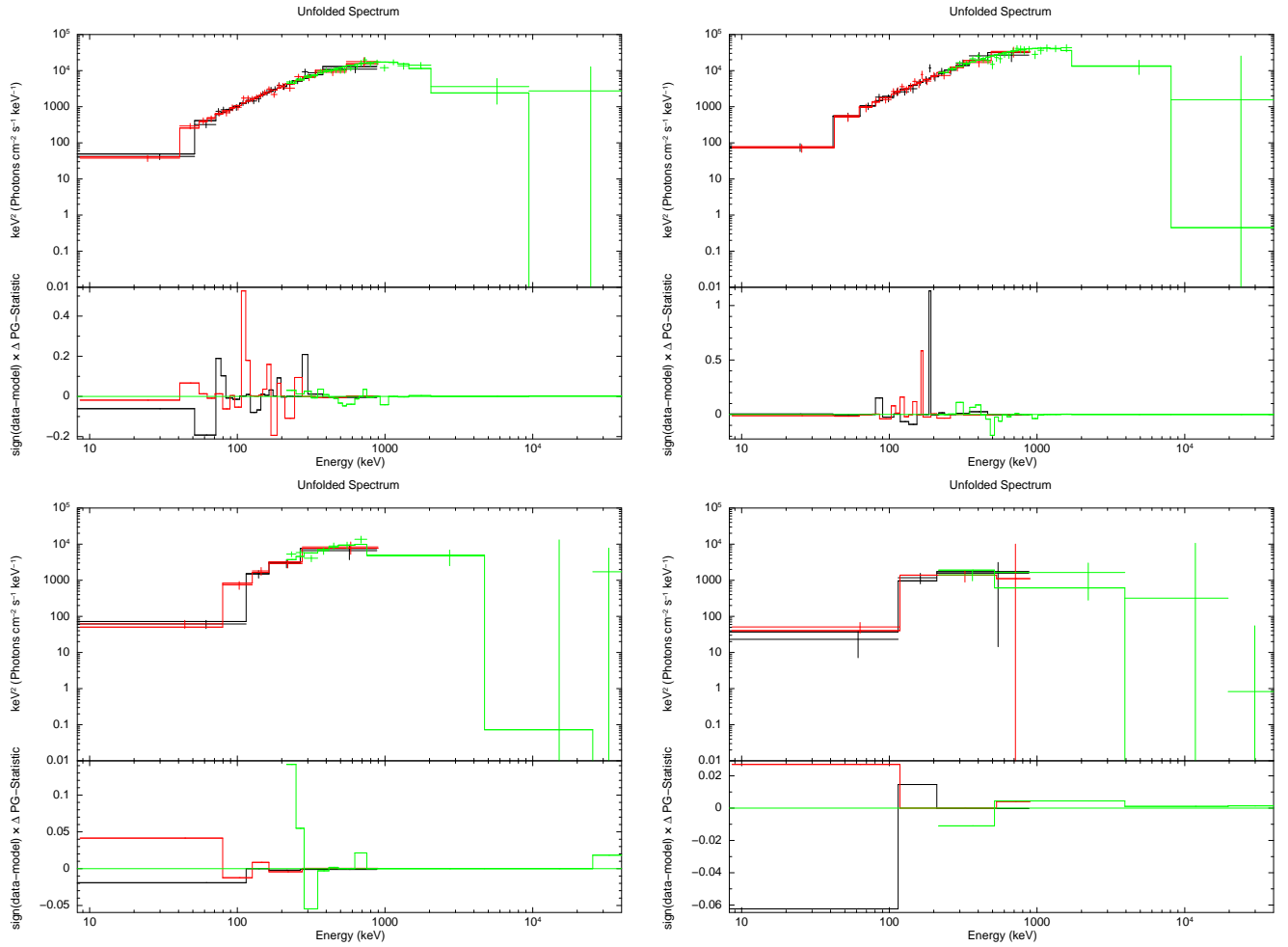


Figure S3: Time-resolved spectra of the burst with the CPL model measured in the time intervals -0.010 – 0.158 s, -0.010 – 0.046 s, 0.046 – 0.102 s and 0.102 – 0.158 s (from left to right). The black points, red points, and green points are the data observed with NaI-n0, NaI-n1, and BGO, respectively. The best-fit parameters can be found in Supplementary Table S1.

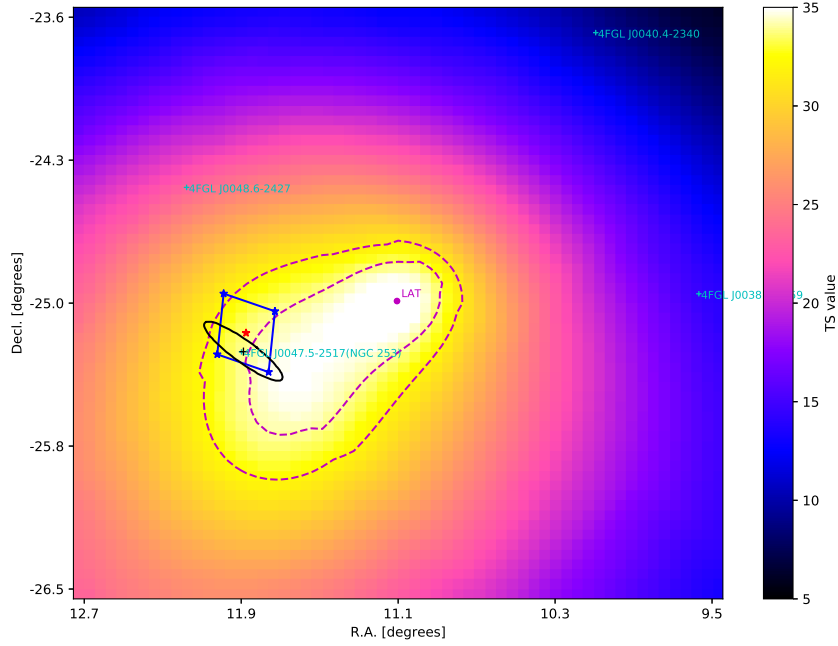


Figure S4: $3 \text{ deg} \times 3 \text{ deg}$ TS map of the GRB 200415A in the energy band 0.1-10 GeV. The green crosses represent the positions of the 4FGL point sources. Black contour depicts the optical emission from the whole NGC 253 with contour level of constant surface brightness of $25 \text{ mag arcsec}^{-2}$ as used in ref.⁴⁴, the black cross represents the the optical centre of the NGC 253. The magenta point indicates the best localization of GRB 200415A. The two magenta dashed circles represent the localization contours of GRB 200415A in 68% and 90% confidence levels. The red (center) and blue stars (corners) represent the IPN error box of GRB 200415A¹⁸. This map has been created for a pixel size of 0.05, smoothed by gaussian kernel ($\sigma = 0.35 \text{ deg}$). The color bar represents the value of TS per pixel.